Closed-Form Jones Matrix of Dual-Polarized Inverted-Vee Dipole Antennas over Lossy Ground

R.A.C. Baelemans[1,2], A.T. Sutinjo[1], P.J. Hall[1], A.B. Smolders[2], M.J. Arts[3], and E. de Lera Acedo[4]

Abstract—This paper presents a closed-form expression for the Jones matrix of a dual-polarized inverted-vee dipole antenna based on the Lorentz reciprocity theorem and the basic rules of electromagnetic refraction. The expression is used to determine the intrinsic cross-polarization ratio (IXR) as function of droop angle, position of the source in the sky, antenna height, frequency, and reflection coefficient of the underlying ground. The expression is verified using full-wave simulations with a Method-of-Moments solver, showing very good agreement. It explains the increase in IXR when the antenna is placed over a perfect electric ground plane. This result is used to explain the polarization properties of the Square Kilometre Array Log-Periodic Antenna (SKALA). Through the Low-Frequency Array Low Band Antenna (LOFAR-LBA) the importance of the size of the ground plane is explained. Finally, design consideration for high polarization purity antennas are discussed.

Index Terms—Polarimetry, radio astronomy, polarization, antenna theory, modeling

I. INTRODUCTION

HIGH polarization purity is necessary in the next generation low-frequency radio telescopes to achieve important science goals, such as the study of the Epoch of Reionization (EoR) [1] and pulsar timing. Low-frequency radio telescopes are generally realized by "aperture arrays", which consist of a large number of dipole-like dual-polarized antennas. Current examples of low-frequency radio telescope aperture arrays include the Low-Frequency Array (LOFAR) [2] in the Netherlands, the Murchison Widefield Array (MWA) [3] in Western Australia, the Long Wavelength Array (LWA) [4] under construction in New Mexico, and the Low-Frequency Aperture Array (LFAA) of the Square Kilometre Array [5] (SKA) which is in the pre-construction phase. Except for the MWA and the LOFAR high band, these examples consist of dual-polarized inverted-vee dipole antennas.

The antenna under consideration for the LFAA of SKA-Low, the SKA Log-periodic Antenna (SKALA), was found to resemble an inverted-vee dipole at its lowest frequency range, since the majority of the radiation is picked up by the supporting boom arms of the antenna instead of the log-periodic elements [6]. It was furthermore found that the use of an electrically small, or no ground plane, greatly reduces its polarization purity at these low frequencies [7] [8].

Corresponding author: Rene Baelemans: renebaelemans@gmail.com
[1]International Centre for Radio Astronomy Research (ICRAR), Curtin University, Bentley, WA 6102, Australia.
[2]Eindhoven University of Technology, The Netherlands.
[3]ASTRON, The Netherlands Institute for Radio Astronomy, The Netherlands.
[4]Cavendish Laboratory, University of Cambridge, United Kingdom.

Although the dielectric soil properties of the proposed site for the LFAA, the Murchison Radio Observatory (MRO), have been determined through measurements, a physical explanation of the increase in polarization purity between deploying the antenna over a perfect electric conductor (PEC) ground plane or over a lossy ground is yet to be made; all of the given interferences so far have been based on Method-of-Moments (MoM) simulation software.

All but one of the previous presented results are based on the use of an infinite PEC ground plane, whereas the other one only considers the polarization purity at boresight [7]. This raises the question how big the ground plane in reality should be to recreate a similar increase in polarization purity. For example, the LOFAR low-band antenna (LBA) and LWA use a individual ground plane, whereas an array-sized ground plane for the SKA-Low is considered. It furthermore raises the question if a dual-polarized inverted-vee dipole antenna with a high polarization purity without the use of a PEC ground plane is feasible.

This paper is organized as follows. Section II is a short review of the IXR. In Section III, the inverted-vee antenna is modeled using the Lorentz reciprocity theorem. This model is used in the case of the standard inverted-vee in Section IV. In Section V, the model and its results are compared to simulations of SKALA. The impact of the size of the ground plane is discussed in Section VI through a comparison of the model and its results with simulations of LOFAR LBA. Finally, Section VII explores design considerations with and without a PEC ground plane.

II. REVIEW OF IXR

The intrinsic cross-polarization ratio (IXR) is introduced by Carozzi and Woan [9] as a fundamental figure-of-merit for assessing polarimetric performance. It is gaining acceptance in low-frequency aperture array applications as is seen by the increasing number of papers utilizing the IXR [6]–[8], [10]–[14]. The IXR provides an upper-bound estimate of the polarimetric error after full polarimetric calibration and it is independent of the chosen coordinate system. The derivation of the IXR is based on Jones matrices [15]. A Jones matrix describes the polarimetric response of a system via $v = Je$, where v indicates the measured voltage vector at the ports of the antenna, J the Jones matrix, and e the 2-element electric field vector of the source in terms of an orthogonal polarization base. The IXR is calculated via

$$\text{IXR}(J) = \left(\frac{e_1 + e_2}{e_1 - e_2}\right)^2 = \left(\frac{\text{cond}(J) + 1}{\text{cond}(J) - 1}\right)^2 \quad (1)$$

where e_1 and e_2 are the eigenvalues of the Jones matrix and where $\text{cond}(\boldsymbol{J})$ denotes the condition number of the Jones matrix under investigation. From the definition of the condition number it follows that a low IXR implies a poor polarimetric response, and a high IXR a good polarimetric response. The IXR is invariant to unitary transformation, e.g. rotation of the coordinate system, because it only depends on the eigenvalues of the Jones matrix.

III. JONES MATRIX OF DUAL-POLARIZED INVERTED-VEE ANTENNAS

To obtain the Jones matrix of any arbitrary antenna configuration, generally a voltage over the antenna ports is applied to calculate the far-field response, i.e. the Jones matrix is derived by using the antenna in transmit mode. This is also the method used when forming the Jones matrix using MoM simulation software, this method is for example used in Section IV to verify the to be derived closed-form expressions.

However, to derive a closed-form expression of the Jones matrix in transmit mode would require the knowledge of the scattered field in the presence of semi-infinite soil, which in turn would require an exact formulation of the Sommerfeld integrals. In the case of a thin wire antenna, such as the one under consideration in this paper, we can assume to know the impressed current distribution over the antenna arms and derive the far-field response due to this impressed current distribution instead.

Knowing this, we will consider the antenna in receive mode instead and apply Lorentz' reciprocity concept [16] [17] to obtain the far-field response of the dual-polarized inverted-vee antenna above a lossy ground, as shown in Fig. 1. The reciprocity concept describes the electromagnetic interaction between two source regions enclosed within a volume V. The relation between the current distributions $(\boldsymbol{\mathcal{J}}^a, \boldsymbol{\mathcal{J}}^b)$ in the source regions (V_a, V_b) and the corresponding fields $(\boldsymbol{E}^a, \boldsymbol{H}^a)$ and $(\boldsymbol{E}^b, \boldsymbol{H}^b)$, respectively, is given by

$$\iint_S \left(\boldsymbol{E}^a \times \boldsymbol{H}^b - \boldsymbol{E}^b \times \boldsymbol{H}^a \right) \cdot \hat{u}_n \, dS =$$
$$\iiint_V \left(\boldsymbol{E}^b \cdot \boldsymbol{\mathcal{J}}^a - \boldsymbol{E}^a \cdot \boldsymbol{\mathcal{J}}^b \right) dV \quad (2)$$

The surface integral, with the surface entirely in free space, vanishes when the volume V is infinite [18]. As a next step, we choose $\boldsymbol{\mathcal{J}}^b$ to be an electric dipole with a dipole moment of one and assume that the distance between both source regions is very large. In this case Eq. (1) can be written in the form

$$\boldsymbol{E}^a(r) \cdot \hat{u}_b = \iiint_{V_a} \left(\boldsymbol{E}^b(\boldsymbol{r}_0 - \boldsymbol{r}) \cdot \boldsymbol{\mathcal{J}}^a(\boldsymbol{r}_0) \right) dV_0 \quad (3)$$

This concept can now be extended to include the reflection from the lossy ground by applying superposition. In this way, the four Jones-matrix elements $(J_{x\theta}, J_{x\phi}, J_{y\theta}, J_{y\phi})$ of
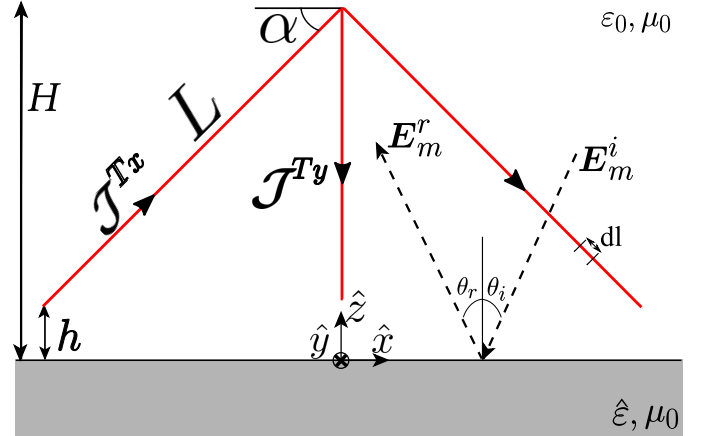

Fig. 1: Graphical representation of a dual-polarized inverted-vee dipole antenna (in red) over a homogeneous lossy ground, showing the droop angle (α), the antenna height (H) and the length of the antenna arms (L). The two dipoles, in the $xz-$ and yz-plane, are completely identical, only rotated by 90° azimuthal angle.

the dual-polarized inverted-vee antenna of Fig.1, with its arms aligned with the $xz-$ and yz-plane, are obtained from [1]

$$J_{nm} = \int_{-L}^{L} \left(\boldsymbol{E}_m^i e^{-j\boldsymbol{k}^i \cdot \boldsymbol{r}_0} + \boldsymbol{E}_m^r e^{-j\boldsymbol{k}^r \cdot \boldsymbol{r}_0} \right) \cdot \boldsymbol{\mathcal{J}}^{Tn} dl \quad (4)$$

where $n \in [x, y]$ (referring to the reaction integral of the antenna arms in the xz-plane or yz-plane) and $m \in [\theta, \phi]$ (referring to the reaction integral to θ-polarized or ϕ-polarized radiation). The incident electric field vectors are given by $\boldsymbol{E}_\theta^i = E_\theta \hat{u}_\theta = E_\theta \left(\cos\theta \cos\phi \hat{u}_x + \cos\theta \sin\phi \hat{u}_y - \sin\theta \hat{u}_z \right)$ and $\boldsymbol{E}_\phi^i = E_\phi \hat{u}_\phi = E_\phi \left(-\sin\phi \hat{u}_x + \cos\phi \hat{u}_y \right)$, where ϕ is the azimuthal angle measured counterclockwise from the x-axis, and where θ is the zenith angle, with $\theta = 0^o$ the zenith point. The incident wave vector is given by $\boldsymbol{k}^i = -k_x \hat{u}_x - k_y \hat{u}_y - k_z \hat{u}_z$. The Euclidean vector $\boldsymbol{r}_0 = r_x \hat{u}_x + r_y \hat{u}_y + r_z \hat{u}_z$ is the vector from the origin to the parameterization over the arms. This parametrization is given by dl, which is integrated in the positive x- or y-direction, for the arms in the xz- and yz-plane respectively. The normalized amplitude of the current distribution over the arms can be approximated by [19],

$$|\boldsymbol{\mathcal{J}}^{Tx}| = |\boldsymbol{\mathcal{J}}^{Ty}| = \sin\left(\frac{f}{f_{res}} \frac{\pi}{2} \left(1 - \frac{|l|}{L} \right) \right) \quad (5)$$

where f/f_{res} denotes the ratio of the frequency of radiation to the half-wave resonance frequency. The reflected wave vector $\boldsymbol{k}^r = -k_x \hat{u}_x - k_y \hat{u}_y + k_z \hat{u}_z$ follows directly from $\boldsymbol{k}^i$ by using $\theta_r = \theta_i$. The reflected field vectors are given by $\boldsymbol{E}_\theta^r = \Gamma_\theta E_\theta \left(\cos\theta \cos\phi \hat{u}_x + \cos\theta \sin\phi \hat{u}_y + \sin\theta \hat{u}_z \right)$ and $\boldsymbol{E}_\phi^r = \Gamma_\phi \boldsymbol{E}_\phi^i$. Since $\boldsymbol{E}_\theta^i$ is purely transverse magnetic polarized (TM) and $\boldsymbol{E}_i^\phi$ is purely transverse electric polarized (TE), their corresponding reflections coefficients (Γ_θ, Γ_ϕ) are well known quantities given by

$$\Gamma_\theta = \frac{Z_{rt} \cos\theta_t - \cos\theta_i}{Z_{rt} \cos\theta_t + \cos\theta_i} \quad \Gamma_\phi = \frac{Z_{rt} \cos\theta_i - \cos\theta_t}{Z_{rt} \cos\theta_i + \cos\theta_t} \quad (6)$$

---

[1]Implicitly assuming the standard time harmonic convention of $e^{j(\omega t - \boldsymbol{k} \cdot \boldsymbol{r})}$.

where Z_{rt} is the ratio between the plane wave impedance in the ground and the free space wave impedance, and where θ_t is the refracted angle as given by Snell's law. These quantities are given by

$$Z_{rt} = \frac{1}{\sqrt{\hat{\varepsilon}_r}} \quad \theta_t = \arcsin\left(\frac{1}{\sqrt{\hat{\varepsilon}_r}}\sin\theta\right) \quad (7)$$

respectively, assuming the underlying ground is non-magnetic. The complex permittivity ($\hat{\varepsilon}_r$) of the ground is given by,

$$\hat{\varepsilon}_r = \varepsilon_r' - j\varepsilon_r'' = \varepsilon_r' - j\frac{\sigma}{\omega\varepsilon_0} \quad (8)$$

where ε_r' is the relative permittivity, σ is the conductivity of the underlying medium, and ε_0 is the free space permittivity. The angular frequency is denoted by ω. For $\hat{\varepsilon}_r = 1$, i.e. free space, $\Gamma_\theta = \Gamma_\phi = 0$ and hence the reflected field is zero. For an infinite PEC ground plane, $\Gamma_\theta = \Gamma_\phi = -1$.

The integrals of the Lorentz reciprocity theorem are solved analytically, and the closed-form expressions of the Jones matrix elements allow calculation of the polarization properties of a dual-polarized inverted-vee dipole antenna over any type of ground which can be characterized by a complex permittivity, even when the relative permittivity and conductivity are frequency dependent. The closed-form solutions of the Jones matrix elements are shown in Appendix A.

IV. POLARIZATION PROPERTIES OF DUAL-POLARIZED INVERTED-VEE DIPOLE ANTENNAS

To test the validity of the closed-form expressions as derived in the previous section, the Jones matrix is also determined using FEKO [20], a MoM simulation tool. The lossy ground is simulated using exact Sommerfeld integrals. Frequency of 50 MHz and a wire radius of $\lambda/4 \times 10^{-3}$ is used for the simulations. FEKO proved to be a reliable simulation tool in the field of (aperture array) antennas, as is concluded from the results in [21]. In resonance the difference between the IXR calculated using simulation and the closed-form expressions is no more than 0.15 dB. Out of resonance this difference stays within a maximum of 1.5 dB for $f < 3f_{res}$, the maximum out of resonance result shown in this paper. It should however be noted that this maximum difference occurs at very high values of the IXR, i.e. it occurs at a highly non-singular Jones matrix only, and is much lower for lower values of the IXR. The very good agreement justifies the derived closed-form solutions.

In this section, the IXR of an antenna at resonance is calculated using the closed-form expressions for three different droop angles, $\alpha = 0^o$ (an orthogonal dipole pair), $\alpha = 45^o$ (the droop angle of the LOFAR LBA), and $\alpha = 80^o$ (the droop angle of the supporting boom arms of the SKALA). At resonance ($f = f_{res}$), the incident and reflected electric field from a flat dipole are exactly in phase in the bore sight direction for $H = \lambda/4$, with $\lambda/4 = L$. The choice is therefore made to keep the feeding point at this constant physical height for all droop angles.

Examining the derived closed-form Jones matrix as given in Appendix A, we can see at the $\phi = 0^o$-cut the Jones matrix simplifies to a diagonal matrix, because $J_{x\phi} = J_{y\theta} = 0$ at
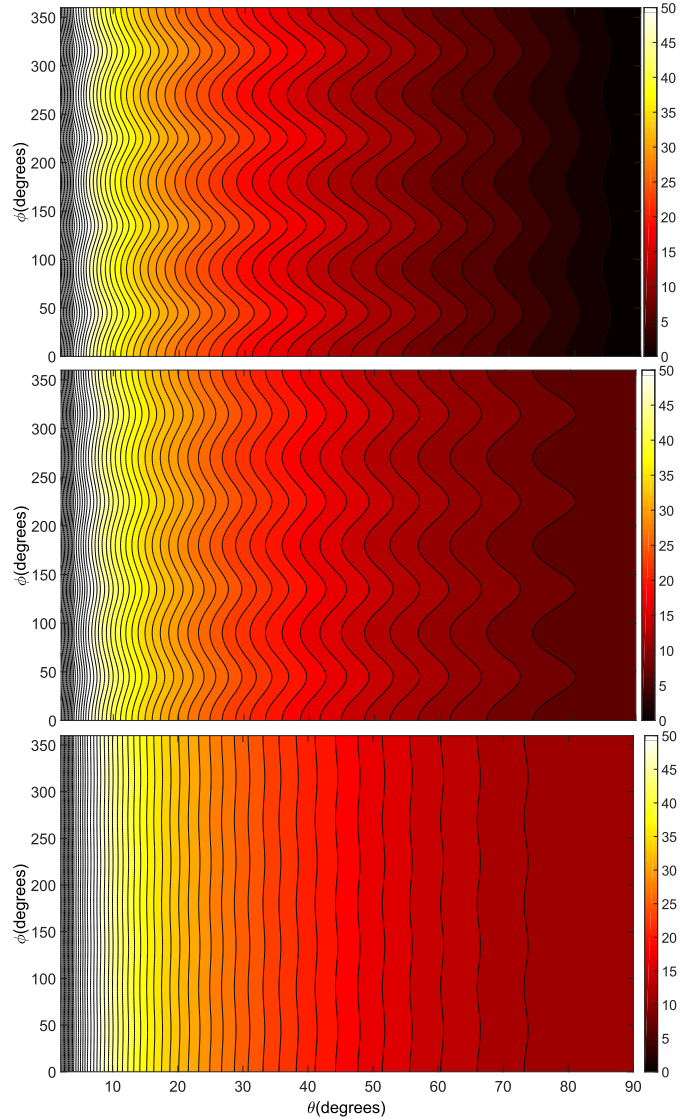

Fig. 2: IXR (dB) of a resonant dual-polarized inverted-vee dipole antenna in free space as function of θ and ϕ for three droop angles, $\alpha = 0^o$ (top), $\alpha = 45^o$ (middle), and $\alpha = 80^o$ (bottom).

this ϕ-cut. $J_{x\phi} = 0$ because $\boldsymbol{E}_\phi$ is purely directed in the y-direction, whereas $J_{y\theta} = 0$ because $\boldsymbol{E}_\theta$ is directed only in the x- and z-direction, where the contribution in the z-direction onto the two y-directed arms exactly cancel due to the opposite polarity at each arm.

A. Free space results

Shown in Fig. 2 are the analytical results for an antenna in free space ($\Gamma_\theta = \Gamma_\phi = 0$). An increase in IXR of up to 10 dB at high zenith (θ) angles is observed when comparing $\alpha = 80^o$ to the flat dipole. Fig. 3 shows the absolute values of $J_{x\theta}$ and $J_{y\phi}$ at the $\phi = 0^o$-cut. For $\alpha = 0^o$, $|J_{y\phi}|$ stays equal for all θ and $|J_{x\theta}|$ decreases with a factor $\cos\theta$, because the two pairs of arms are completely orthogonal to any z-directed fields. However, for non-flat dipoles, this z-directed field is picked up by the arm directed in the xz-plane, which can be seen in Fig. 3 as a slower decrease in $J_{x\theta}$, which in turn explains the increase in IXR for higher droop angles.
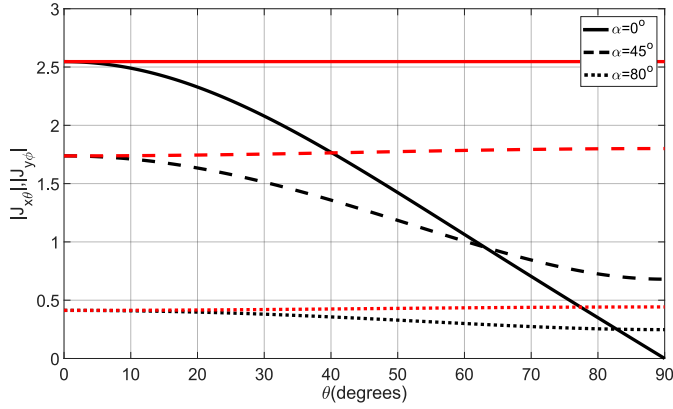
Fig. 3: Absolute values of $J_{x\theta}$ (black lines) and $J_{y\phi}$ (red lines) of a resonant dual-polarized inverted-vee dipole antenna as function of θ at the $\phi = 0^o$-cut for the three droop angles, 0° (solid), 45° (large dash), and 80° (small dash). In free space.

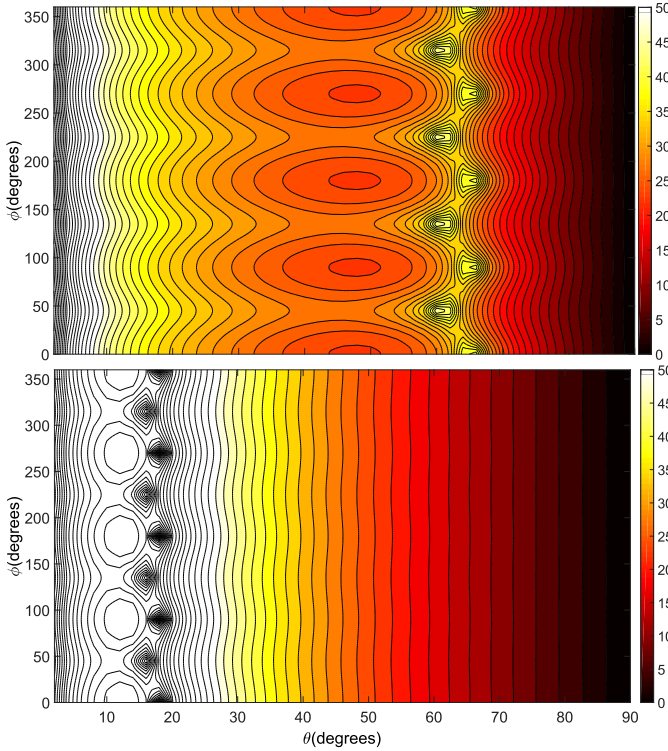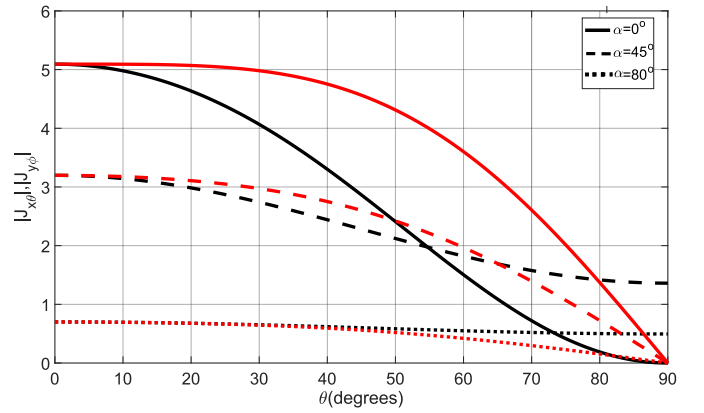Fig. 5: Absolute values of $J_{x\theta}$ (black lines) and $J_{y\phi}$ (red lines) of a resonant dual-polarized inverted-vee dipole antenna over a PEC ground plane as a function of θ. All at the $\phi = 0^o$-cut, for three droop angles, 0° (solid), 45° (large dash), and 80° (small dash).

Fig. 4: IXR (dB) of a resonant dual-polarized inverted-vee dipole antenna over a PEC ground plane ($H = \lambda/4$) as function of θ and ϕ, $\alpha = 45^o$ (top) and $\alpha = 80^o$ (bottom).

B. PEC ground plane results

Fig. 4 shows the IXR over a PEC ground plane ($\Gamma_\theta = \Gamma_\phi = -1$) for $\alpha = 45^o$ and $\alpha = 80^o$ respectively. The IXR of the flat dipole pair is the same as the free space result of Fig. 2 and hence not shown. The Jones matrices for $\alpha = 0^o$ are unitary transforms of each other in free space and over the PEC ground plane, since the reflection coefficients of the PEC ground plane are equal for both polarizations, and both arms are insensitive to z-directed radiation.

The ground plane case shows an increase in IXR in comparison with the free space results of Fig. 2 and the presence of secondary maxima in the IXR. The cause of the secondary IXR

peaks is explained by plotting $|J_{x\theta}|$ and $|J_{y\phi}|$ as a function of θ for $\phi = 0^o$. From Fig. 5 it is concluded that a maximum in IXR occurs when the Jones matrix satisfies

$$|J_{x\theta}| = |J_{y\phi}| \tag{9}$$

and that the difference between the two variables is a good measure of the IXR at $\phi = 0^o$, a result which was already found by Fiorelli et al. [12]. The most eminent example of a secondary maximum is the $\alpha = 45^o$ case of Fig. 5, which satisfies (9) at $\theta = 65^o$, coinciding with the secondary maximum in the IXR of the top graph of Fig. 4. One can see, both for free space and over the PEC ground plane, that for larger droop angles the absolute values of $J_{x\theta}$ and $J_{y\phi}$ diverge more slowly, which is the cause of the increase in IXR. The flat dipole pair ($\alpha = 0^o$) shows a difference in the shape of $|J_{x\theta}|$ and $|J_{y\phi}|$ between Fig. 3 and Fig. 5 but still result in exactly the same IXR due to an unitary transformation (multiplication by an array factor of $\sin(\pi/2 \cos\theta)$) of the Jones matrix.

The cause of the higher IXR and secondary maxima can be explained by the boundary condition of the electric field vector across a perfect conductor. Electric field component parallel to the PEC ground plane changes polarity during reflection, whereas electric field component normal to the PEC ground plane do not change polarity. As a result, the combination of the incident and the reflected field components in the normal and parallel direction will constructively or destructively interfere at different heights and zenith angles. For $\phi = 0^o$, for which the Jones matrix elements are shown in Fig. 5, $\boldsymbol{E}_\phi$ is parallel for all zenith angles, whereas $\boldsymbol{E}_\theta$ becomes increasingly normal for increasing zenith angles, and as a results $|J_{x\theta}|$ is no longer zero at $\theta = 90^o$. Since the ratio between parallel- and normal-directed currents over the arms is a function of the droop angle the position of the secondary maximum similarly is a function of the droop angle.

C. Lossy ground results

The free space case and the PEC ground plane case have shown that the azimuthal angle dependence of the IXR is purely a geometrical one. Since the reflection coefficients also
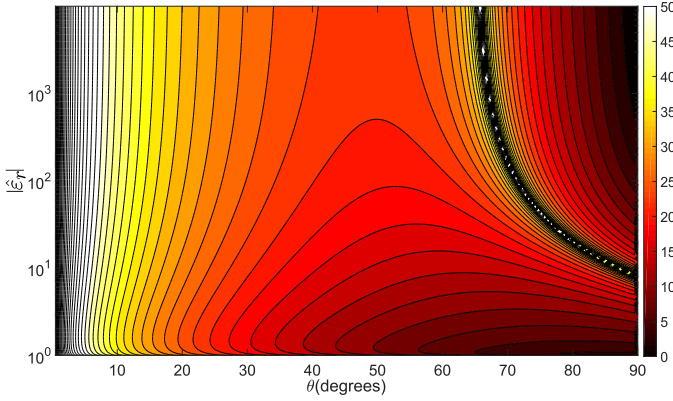
Fig. 6: IXR (dB) of a resonant dual-polarized inverted-vee dipole antenna over a lossy ground as function of the zenith angle and the dielectric ground properties given by $|\hat{\varepsilon}_r|$. The $\phi = 0^o$-cut, $\alpha = 45^0$, $H = \lambda/4$ and $\varepsilon_r' = 1$.
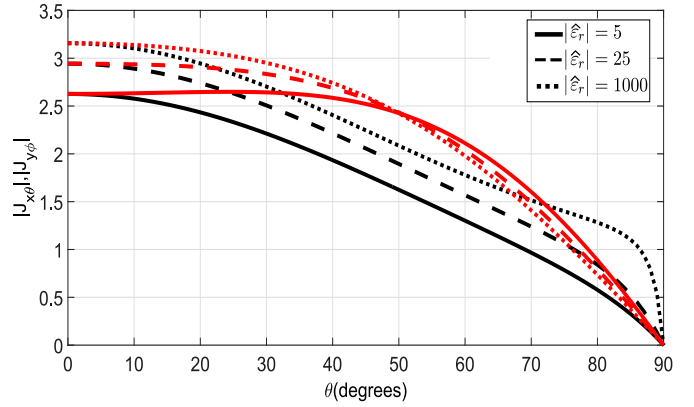

Fig. 7: Absolute values of $J_{x\theta}$ (black lines) and $J_{y\phi}$ (red lines) of a resonant dual-polarized inverted-vee dipole antenna as function of θ for three dielectric ground properties, $|\hat{\varepsilon}_r| = 5$ (solid), $|\hat{\varepsilon}_r| = 25$ (large dash), and $|\hat{\varepsilon}_r| = 1000$ (small dash). The $\phi = 0^o$-cut, droop angle of $\alpha = 45^o$ antenna height of $H = \lambda/4$, and $\varepsilon_r' = 1$.

only depend on the incident zenith angle, a single azimuthal cut is adequate for illustration of the IXR over a lossy ground. Fig. 6 shows the IXR (dB) at the $\phi = 0^o$-cut of an antenna with a droop angle of 45° as function of the absolute value of the complex permittivity ($|\hat{\varepsilon}_r|$) with the real part $\varepsilon_r' = 1$.

As expected, a low conducting medium resembles the IXR in free space and a high conducting medium resembles the IXR over a PEC ground plane, compare Fig. 6 with the $\alpha = 45^o$ case of Fig. 2 and Fig. 4. The transition between the two extremes is a smooth one, for increasing $|\hat{\varepsilon}_r|$ the secondary maximum moves from high zenith angles towards the position for over the PEC ground plane, a zenith angle of $\theta = 65^o$ for the antenna under consideration here. The IXR is mostly dependent on $|\hat{\varepsilon}_r|$ and to a lesser degree on the angle of the complex permittivity, which is of small influence at small values of $|\hat{\varepsilon}_r|$.

By plotting $|J_{x\theta}|$ and $|J_{y\phi}|$ as function of the zenith angle, as is shown in Fig. 4 for three values of $|\hat{\varepsilon}_r|$, we can further explore the effect of a lossy ground. A deformation of the Jones matrix diagonals as a result of the complex permittivity and now complex and unequal reflection coefficients can be seen, especially for $|J_{x\theta}|$. For increasing values of $|\hat{\varepsilon}_r|$ both reflection coefficients increase towards their PEC ground plane value of $\Gamma_\theta = \Gamma_\phi = -1$. From these results we can conclude that the increase in IXR for increasing values of $|\hat{\varepsilon}_r|$ is mostly due to an increase in $|\Gamma_\theta|$ and $|\Gamma_\phi|$.

The results in this section have shown that generally an increase in the polarization purity of a dual-polarized inverted-vee dipole antenna as expressed by the IXR can be expected by deploying a PEC ground plane over lossy ground.

V. Square Kilometre Array Log-periodic antenna (SKALA)

Having derived closed-form expressions of the polarization properties of dual-polarized inverted-vee dipole antennas and after gaining an understanding of the effect of the dielectric properties of the ground on the polarization purity we can now make the comparison between a dual-polarized inverted-vee dipole antenna and the Square Kilometre Array Log-periodic antenna (SKALA).

The SKALA can be considered an inverted-vee dipole at its lowest frequency range, because the majority of the radiation is picked up by the supporting antenna arms instead of the bow-tie and log-periodic parts [6]. Deploying no ground plane greatly reduces the IXR at these frequencies [7]. The supporting arms of the SKALA are 1.371 m long. However, the presence of the bow-tie at the bottom effectively enlarges this resonant length to 1.670 m resulting in a resonance frequency of 45.0 MHz. The L-shape of the "inverted-vee" arms due to the bow-tie at the end of the supporting boom arms is not taken into account by our expressions. The feeding point is placed at $H = 1.804$ m which is 0.27λ at resonance. Two types of infinite grounds are considered here, a PEC ground plane, and the soil of the Murchison Radio Observatory (MRO) [22], near the proposed site of the SKA-Low. The dielectric properties of this type of soil have been measured over a wide range of frequencies and moisture contents of the soil. For this analysis we assume the case for 2% moisture content for which the dielectric variables at a selection of frequencies are shown in Table. I.

The IXR (dB) of SKALA at the $\phi = 0^o$-cut, as function of frequency and zenith angle, simulated using a FEKO model of SKALA [13] is shown in Fig. 8, over the MRO soil and over an infinite PEC ground plane respectively. Deploying a PEC ground plane results in a significant improvement of the IXR of the SKALA below 70 MHz, as can be concluded from the difference between the two results This results is one of the main reasons for the current plan to deploy an array-sized PEC ground plane beneath the SKA-Low arrays.

Now, we want to understand and explain this increase in IXR using the expressions derived in this paper. For this purpose, the IXR of an inverted-vee antenna with the dimensions of the supporting boom arms of the SKALA is calculated using the closed-form expressions. The results are shown in Fig. 9 over the lossy MRO soil and the infinite PEC ground plane respectively. Comparing the IXR of the SKALA and inverted-vee antenna, we see that both show an increase when deploying a PEC ground plane. This result is consistent with the assumption of the inverted-vee behavior of the SKALA

TABLE I: Measured relative permittivity ε'_r and conductivity σ of the MRO soil with a 2% moisture content at spot frequencies [22].

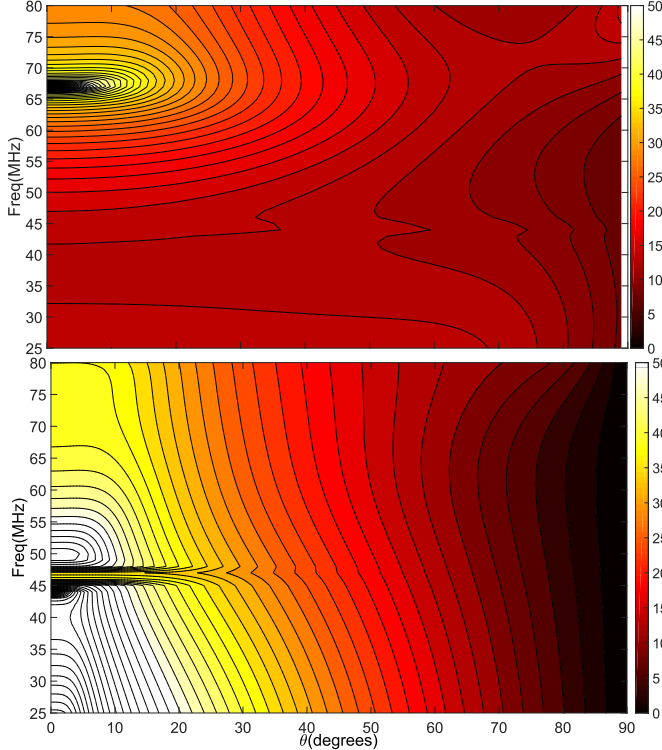|	50 MHz	150 MHz	250 MHz	350 MHz
ε'_r	6.40	5.29	4.98	4.84
σ (S/m)	0.0912	0.018	0.023	0.028
$|\hat{\varepsilon}_r|$	26.90	14.30	11.47	10.31

Fig. 8: Simulated IXR (dB) of SKALA as a function of θ and frequency, over 2% moisture content MRO soil (top) and an infinite PEC ground plane (bottom). Using a FEKO model for $\phi = 0^o$.

below 70 MHz.

However, a significant difference between the two results can be seen, most notably the lack of secondary maxima in the IXR of the SKALA over a PEC ground plane. This can be attributed to the fact that the log-periodic and bow-tie elements are connected to the supporting boom arm that forms the opposite polarization direction, intuitively introducing a raw polarization error. As a result, the derivation stating that the Jones matrix simplifies to a diagonal matrix at $\phi = 0^o$ as was suggested in section IV no longer holds. The expressions derived in this paper hence do not replicate the behavior of the SKALA when it comes to its polarization properties, but predict the correct trend for the PEC ground plane.

The decrease in IXR of the inverted-vee dipole antenna over soil is less severe. This suggests designing a dual-polarized inverted-vee dipole antenna with a high polarization purity without the aid of a PEC ground plane is feasible, although a PEC ground plane will still increase its polarization purity.

VI. GROUND PLANE SIZE

Knowing that deploying an infinite PEC ground plane can greatly increase the polarization purity of the standard
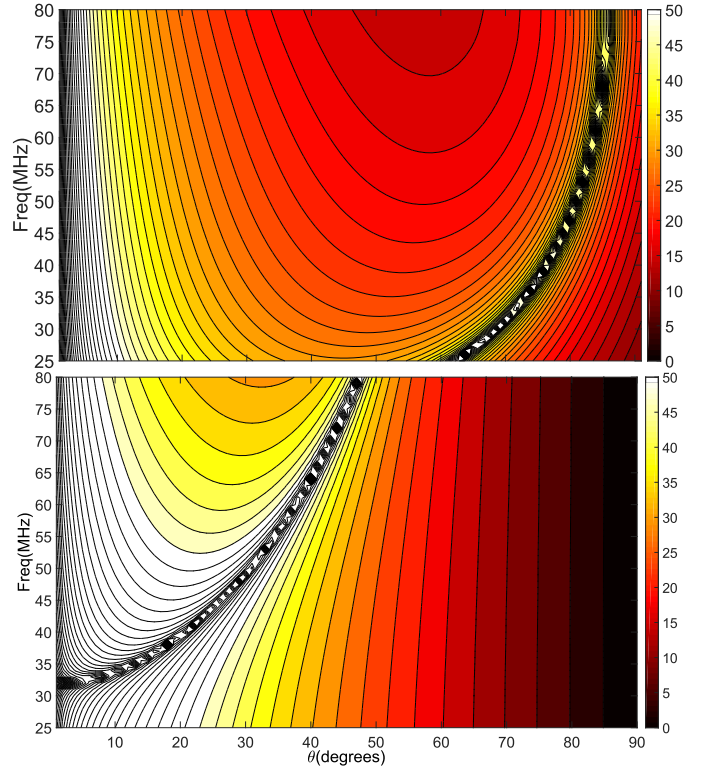

Fig. 9: Calculated IXR (dB) of the inverted-vee approximation of SKALA, over 2% moisture content MRO soil (top), and over an infinite PEC ground plane (bottom). Using the closed-form expressions for $\phi = 0^0$.

inverted-vee and the SKALA raises the question how big a realistic ground plane should be. The trade-off between individual ground planes, such as deployed under the LOFAR LBA and LWA antennas, and array-sized ground planes as under consideration for the SKA-Low stations, is an important one. As an example, we consider the case of the LOFAR LBA.

The LOFAR LBA is an aperture array radio telescope consisting of dual-polarized inverted-vee dipole antennas with a droop angle of 45°. The length of its arms is 1.38 m each, which results in a resonance frequency of 54.3 MHz. The feeding point is elevated to $H = 1.706$ m, which is 0.31λ at resonance. The antenna is placed over a 3×3 m square metallic ground plane. The arms are placed in the direction of the corners of the ground plane. The underlying soil is assumed to have a relative dielectric constant of 10, and a conductivity of 0.03 S/m at 50 MHz ($|\hat{\varepsilon}_r| = 68.52$) [23].

The top graph of Fig. 10 shows the IXR (dB) of LOFAR LBA over only the soil, i.e. without a ground plane, calculated using the closed-form expressions for a lossy ground as derived in this paper. The middle graph shows the IXR (dB) from a WIPL-D model [23], assuming a 3-by-3 m metallic ground plane over the soil, and the bottom graph shows the IXR (dB) over the infinite PEC ground plane as derived in this paper. The secondary maxima in the IXR of the simulated LOFAR LBA occur at a zenith (θ) angle of 85° but are omitted because of the low resolution in zenith (θ) angle of this simulation. The small ground plane shows only a marginal increase in IXR compared to the IXR over only the soil, and secondary maxima at nearly the same zenith angle. This can
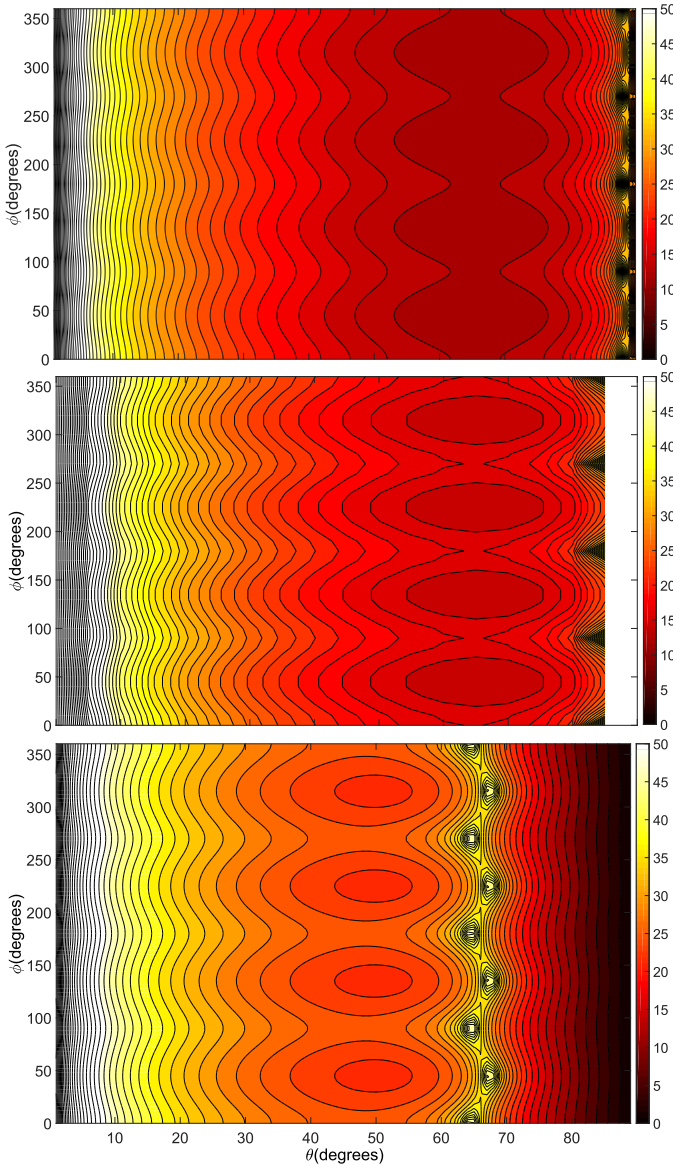
Fig. 10: Calculated IXR (dB) of LOFAR LBA over the lossy dielectric soil using the model derived in this paper (top). IXR (dB) simulation results of LOFAR LBA with a small PEC ground plane (middle). Calculated IXR (dB) of LOFAR LBA using the model assuming an infinite PEC ground plane (bottom). All at 50 MHz.

be attributed to the small size of the used ground plane at LOFAR LBA, dimensioned at half a wavelength.

The infinite PEC ground plane case however shows an IXR contour with secondary IXR peaks at lower zenith angles in comparison with the soil case, and a strong increase in the IXR. This result strongly suggests deploying larger individual- or a bigger single ground planes underneath the (core site of) LOFAR LBA as it will significantly increase its polarization purity. This result equally well applies to the standard inverted-vee dipole antenna and the SKALA, where also ground planes of several wavelengths in size should be considered.

VII. DESIGN CONSIDERATIONS

The previous results have shown that a very high polarization purity can be realized by deploying a PEC ground plane

underneath the antenna. This however raises the question if a sufficiently high polarization purity can also be achieved without deploying this PEC ground plane, i.e. by deploying the antenna over just the lossy soil. To answer this question, we utilize the the most accurate soil model available, the previously used MRO soil model with a moisture content of 2%. We will mimic the polarization requirements of the SKA-Low radio-telescope only limiting the frequency range to $(1:3)$ to keep within the 1.5 dB IXR difference between simulation and model as set out in Section IV, i.e. we will consider the IXR over a frequency range of $50-150$ MHz and a field-of-view (FoV) of 45° zenith angle. Only the worst, i.e. the minimal, IXR over this frequency band and FoV is of interest, since this effectively limits the polarization performance. This section discusses purely a polarization purity exercise, a realistic design obviously needs to account for more parameters, such as gain, efficiency, beam pattern, and impedance.

Shown in the top graph of Fig. 11 is the minimal value of the IXR (dB) over the FoV and frequency range as function of two design parameters, the length of the antenna arms (L) and the droop angle (α). The IXR_{min} for each design is calculated using the closed-form expressions. As in previous sections, the choice is made to keep the height of the antenna exactly at a quarter wavelength of the resonance frequency, i.e. $H = L$. From the result given in Fig. 11 we can conclude that a high polarization purity in the antenna over soil case is achieved by choosing a large droop angle and short length antenna arms. As an example of a realistic design, an antenna with a droop angle of $\alpha = 65^o$ and antenna arms of $L = 1$ m has got an IXR of over 15 dB for the entire FoV and frequency range.

As a comparison, the bottom graph of Fig. 11 shows the minimal value of the IXR (dB) as function of the same parameters now after deploying an infinite PEC ground plane. Once again the minimal value of the IXR (dB) over the FoV and frequency band is calculated using the closed-form expressions as derived in this paper. Consistent with previous results we can conclude that for short dipoles deploying a PEC ground plane results in an increase in polarization purity. For the case of a droop angle of $\alpha = 65^o$ and antenna arms of 1 m, the PEC ground plane has got an IXR of over 20 dB for the entire FoV and frequency range.

However, for wavelengths short compared to the dipole length, i.e. long inverted-vee dipoles, a full cancellation of the incident and reflected fields for one of the polarization states occurs within the FoV. As can be seen in the bottom graph of Fig. 11 this results in the worst possible polarimetric response, an IXR of zero dB. This cancellation does not occur in the case of a lossy ground since the reflection coefficients are complex and unequal.

This section has shown the strength of the closed-form expressions of the Jones matrix elements, since it allows for a rapid calculation of the polarization properties. The derived expression can very well be used as a first design step for antenna engineers faced with the challenge of designing antennas with a high polarization purity.
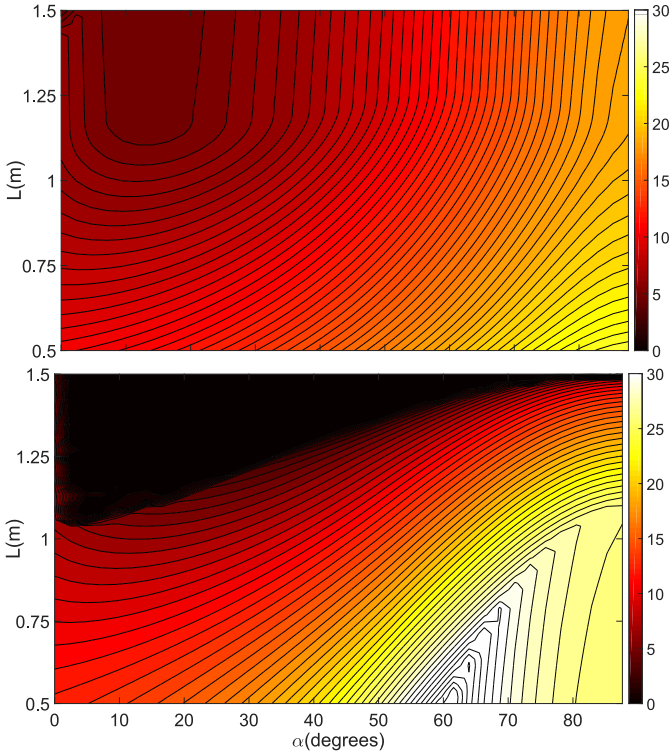
Fig. 11: IXR$_{\min}$ (dB) of a dual-polarized inverted-vee dipole antenna as function of the length of the arms (L) and the droop angle (α) deployed over the 2% moisture content MRO soil (top graph) and over an infinite PEC ground plane (bottom graph). For a FoV of 45° zenith angle, a frequency range of $50 - 150$ MHz and an antenna height of $H = L$. (Notice the difference in the dB scale of these graphs ($0 - 30$ dB) in comparison with previous graphs ($0 - 50$ dB).)

VIII. CONCLUSION

Closed-form expressions describing the polarization properties of dual-polarized inverted-vee dipole antennas over lossy ground have been derived. These expressions have been verified as accurate using full-wave simulations. The closed-form expressions give a good understanding of the underlying physical phenomena that influence the IXR of dual-polarized inverted-vee antennas. Using these closed-form expressions and the resulting IXR, one can justify and understand the necessity of the use of highly conducting ground planes in radio astronomy applications based on dual-polarized inverted-vee dipole antennas. The comparison between the derived closed-form expressions and the SKALA explains the increase in IXR based on the inverted-vee behavior at low frequencies of the SKALA with a PEC ground plane deployed. Through the comparison of the derived closed-form expressions and the LOFAR LBA, which has a small ground plane, we concluded that a significant improvement in its polarization purity can be achieved by deploying a bigger ground plane, a result which can be generalized to all dual-polarized inverted-vee dipole antenna based antennas. Finally, we showed that a high polarization purity can also be achieved over the realistic MRO soil without the need of a PEC ground plane. This furthermore demonstrates that the derived closed-form expressions can be used as a first design step for antennas with a high polarization purity, because the derived closed-form expressions give both

a better understanding and near-instant results relative to full-wave EM simulations.

APPENDIX

The closed-form solution of the Jones matrix

$$J_{x\theta} = I_\theta \cos\theta \cos\phi \cos\alpha + II_\theta \sin\theta \sin\alpha \tag{10a}$$

$$J_{x\phi} = -I_\phi \sin\phi \cos\alpha \tag{10b}$$

$$J_{y\theta} = III_\theta \cos\theta \sin\phi \cos\alpha + IV_\theta \sin\theta \sin\alpha \tag{10c}$$

$$J_{y\phi} = III_\phi \cos\phi \cos\alpha \tag{10d}$$

where (with $m \in [\theta, \phi]$)

$$I_m = e^{jC+jD} \left[f_1 + f_2 + f_3 + f_4 \right] + \Gamma_m e^{-jC-jD} \left[f_5 + f_6 + f_7 + f_8 \right] \tag{11a}$$

$$II_m = e^{jC+jD} \left[f_1 - f_2 + f_3 - f_4 \right] - \Gamma_m e^{-jC-jD} \left[f_5 - f_6 + f_7 - f_8 \right] \tag{11b}$$

where

$$f_1 = \frac{1 - e^{j(-C-\gamma+A)}}{-C - \gamma + A} \quad f_5 = \frac{1 - e^{j(C-\gamma+A)}}{C - \gamma + A} \tag{12a}$$

$$f_2 = \frac{1 - e^{j(-C-\gamma-A)}}{-C - \gamma - A} \quad f_6 = \frac{1 - e^{j(C-\gamma-A)}}{C - \gamma - A} \tag{12b}$$

$$f_3 = \frac{1 - e^{j(-C+\gamma+A)}}{-C + \gamma + A} \quad f_7 = \frac{1 - e^{j(C+\gamma+A)}}{C + \gamma + A} \tag{12c}$$

$$f_4 = \frac{1 - e^{j(-C+\gamma-A)}}{-C + \gamma - A} \quad f_8 = \frac{1 - e^{j(C+\gamma-A)}}{C + \gamma - A} \tag{12d}$$

where

$$A = \gamma \cos\alpha \sin\theta \cos\phi \tag{13a}$$

$$B = \gamma \cos\alpha \sin\theta \sin\phi \tag{13b}$$

$$C = \gamma \sin\alpha \cos\theta \tag{13c}$$

$$D = \gamma \left(\frac{4H}{\lambda} - \sin\alpha \right) \cos\theta \tag{13d}$$

and where

$$\gamma = \frac{f}{f_{res}} \frac{\pi}{2} \tag{14}$$

Furthermore, $III_m = I_m|_{A=B}$ and $IV_m = II_m|_{A=B}$.

REFERENCES

[1] S. Zaroubi, "The Epoch of Reionization," in *The First Galaxies*, ser. Astrophysics and Space Science Library. Springer Berlin Heidelberg, 2013, vol. 396, pp. 45–101.

[2] M. de Vos, A. Gunst, and R. Nijboer, "The LOFAR Telescope: System Architecture and Signal Processing," *Proceedings of the IEEE*, vol. 97, no. 8, pp. 1431–1437, Aug 2009.

[3] S. J. Tingay, R. Goeke, J. D. Bowman, D. Emrich, S. M. Ord, D. A. Mitchell, M. F. Morales, T. Booler, B. Crosse, R. B. Wayth, C. J. Lonsdale, S. Tremblay, D. Pallot, T. Colegate, A. Wicenec, N. Kudryavtseva, W. Arcus, D. Barnes, G. Bernardi, F. Briggs, S. Burns, J. D. Bunton, R. J. Cappallo, B. E. Corey, A. Deshpande, L. Desouza, B. M. Gaensler, L. J. Greenhill, P. J. Hall, B. J. Hazelton, D. Herne, J. N. Hewitt, M. Johnston-Hollitt, D. L. Kaplan, J. C. Kasper, B. B. Kincaid, R. Koenig, E. Kratzenberg, M. J. Lynch, B. Mckinley, S. R. Mcwhirter, E. Morgan, D. Oberoi, J. Pathikulangara, T. Prabu, R. A. Remillard, A. E. E. Rogers, A. Roshi, J. E. Salah, R. J. Sault, N. Udaya-Shankar, F. Schlagenhaufer, K. S. Srivani, J. Stevens, R. Subrahmanyan, M. Waterson, R. L. Webster, A. R. Whitney, A. Williams, C. L. Williams, and J. S. B. Wyithe, "The Murchison Widefield Array: The Square Kilometre Array Precursor at Low Radio Frequencies," *Publications of the Astronomical Society of Australia*, vol. 30, 2013.

[4] S. Ellingson, T. Clarke, A. Cohen, J. Craig, N. Kassim, Y. Pihlstrom, L. Rickard, and G. Taylor, "The Long Wavelength Array," *Proceedings of the IEEE*, vol. 97, no. 8, pp. 1421–1430, Aug 2009.

[5] P. Dewdney, P. Hall, R. Schilizzi, and T. Lazio, "The Square Kilometre Array," *Proceedings of the IEEE*, vol. 97, no. 8, pp. 1482–1496, Aug 2009.

[6] E. de Lera Acedo, B. Fiorelli, and M. Arts, "Polarization performance of log-periodic antennas on top of different types of ground plane; the SKA-low instrument case," in *Antennas and Propagation (EuCAP), 2015 9th European Conference on*, April 2015, pp. 1–4.

[7] B. Fiorelli and E. de Lera Acedo, "Polarization performance of the SKA Low Frequency Aperture Array station," in *International Conference on Electromagnetics in Advanced Applications (ICEAA)*, Aug 2014, pp. 726–729.

[8] B. Fiorelli, E. de Lera Acedo, M. Arts, G. Virone, and J. bij de Vaate, "Polarization performances and antenna misalignment errors for aperture arrays: SKA-low AAVS0.5 case," in *International Conference on Electromagnetics in Advanced Applications (ICEAA)*, Sept 2013, pp. 972–975.

[9] T. Carozzi and G. Woan, "A Fundamental Figure of Merit for Radio Polarimeters," *IEEE Transactions on Antennas and Propagation*, vol. 59, no. 6, pp. 2058–2065, June 2011.

[10] A. Sutinjo and P. Hall, "Intrinsic Cross-Polarization Ratio of Dual-Linearly Polarized Antennas for Low-Frequency Radio Astronomy," *IEEE Transactions on Antennas and Propagation*, vol. 61, no. 5, pp. 2852–2856, May 2013.

[11] A. Sutinjo and P. Hall, "Antenna Rotation Error Tolerance for a Low-Frequency Aperture Array Polarimeter," *IEEE Transactions on Antennas and Propagation*, vol. 62, no. 6, pp. 3401–3406, June 2014.

[12] B. Fiorelli, M. Arts, G. Virone, E. de Lera Acedo, and W. van Cappellen, "Polarization analysis and evaluation for radio astronomy aperture array antennas," in *Antennas and Propagation (EuCAP), 2013 7th European Conference on*, April 2013, pp. 461–465.

[13] E. de Lera Acedo, N. Razavi-Ghods, N. Troop, N. Drought, and A. Faulkner, "SKALA, a log-periodic array antenna for the SKA-low instrument: design, simulations, tests and system considerations," *Exp. Astronomy*, 2015, 39:567-594. doi: 10.1007/s10686-015-9439-0.

[14] B. Fiorelli and E. de Lera Acedo, "On the simulation and validation of the Intrinsic Cross-Polarization Ratio for antenna arrays devoted to low frequency radio astronomy," in *Antennas and Propagation (EuCAP), 2014 8th European Conference on*, April 2014, pp. 2361–2364.

[15] R. C. Jones, "A New Calculus for the Treatment of Optical Systems I. Description and Discussion of the Calculus,," *Journal of the Optical Society of America.*, no. 7, pp. 488–493.

[16] R. Harrington, *Time-Harmonic Electromagnetic Fields*. Wiley-Interscience, 2001, chapter 3.

[17] W. Weeks, *Antenna Engineering*. McGraw-Hill, 1968, chapter 8, Section 1.10.

[18] H. Lorentz, "The theorem of Poynting concerning the energy in the electromagnetic field and two general propositions concerning the propagation of light," *Amsterdammer Akademie der Wetenschappen*, no. 4, p. 176, 1896.

[19] C. Balanis, *Antenna Theory: Analysis and Design*. Wiley, 2005.

[20] *FEKO 7.0*, EM Software & Systems - Stellenbosch South Africa Std.

[21] T. Colegate, A. Sutinjo, P. Hall, S. Padhi, R. Wayth, J. bij de Vaate, B. Crosse, D. Emrich, A. Faulkner, N. Hurley-Walker, E. de Lera Acedo, B. Juswardy, N. Razavi-Ghods, S. Tingay, and A. Williams, "Antenna array characterization via radio interferometry observation of astronomical sources," in *Antenna Measurements Applications (CAMA), 2014 IEEE Conference on*, Nov 2014, pp. 1–4.

[22] A. T. Sutinjo, T. M. Colegate, R. B. Wayth, P. J. Hall, E. de Lera Acedo, T. Booler, A. J. Faulkner, L. Feng, N. Hurley-Walker, B. Juswardy, S. K. Padhi, N. Razavi-Ghods, M. Sokolowski, S. J. Tingay, and J. G. B. de Vaate, "Characterization of a Low-Frequency Radio Astronomy Prototype Array in Western Australia," *IEEE Transactions on Antennas and Propagation*, vol. 63, no. 12, pp. 5433–5442, Dec 2015.

[23] M. Arts, "EM-simulations of the final design of the LOFAR low band antenna," ASTRON internal report: personal communication M.J. Arts, arts@astron.nl.